DOI: 10.1002/ejic.200901120

Protonation of Cp*M(dppe)H Hydrides: Peculiarities of the Osmium Congener

Pavel A. Dub,[a,b] Oleg A. Fillipov,[a] Gleb A. Silantyev,[a] Natalia V. Belkova,*[a] Jean-Claude Daran,[b] Lina M. Epstein,[a] Rinaldo Poli,*[b,c] and Elena S. Shubina*[a]

Keywords: Osmium / Hydrido ligand / Proton transfer / Hydrogen bonds / Density functional calculations

The interaction between Cp*OsH(dppe) (**1**) and a series of proton donors (HA) of increasing strength [indole, CFH_2CH_2OH (MFE), CF_3CH_2OH (TFE), $(CF_3)_2CHOH$ (HFIP), *p*-nitrophenol, and $HBF_4{\cdot}Et_2O$] has been investigated experimentally by variable temperature IR and NMR spectroscopy in solvents with different coordinating abilities (alkanes, dichloromethane and their mixtures) and computationally at the DFT/B3PW91 level using different models. Both the IR and NMR spectroscopic data for the interaction with weak proton donors conform to the criteria of M–H···H-A bond formation. Theoretical calculations, however, indicate an asymmetric bifurcated interaction with a significant contribution from the metal atom, which is greater than that previously found for the corresponding Fe system. The basicity factor of **1** (E_j = 1.47) is greater than those of the Ru (1.39) and Fe (1.35) congeners, in agreement with previous studies on other compound families. The kinetic product of proton transfer, *cis*-$[Cp^*Os(H)_2(dppe)]^+X^-$, which is selectively obtained at low temperatures, irreversibly rearranges to *trans*-$[Cp^*Os(H)_2(dppe)]^+X^-$ upon warming to >230 K. The latter compound with X = BF_4 has been crystallographically characterized. The activation enthalpy of the isomerization process ($\Delta H^{\neq}$ = 21.5 ± 1.0 kcal mol^{-1}), obtained from kinetics investigation by ^{1}H NMR in the 240–260 K range, is identical within experimental error to those previously reported for the $M(\eta^2\text{-}H_2)^+BF_4^- \rightarrow$ *trans*-$M(H)_2{}^+BF_4^-$ isomerization process of the iron and ruthenium analogues. The activation entropy ($\Delta S^{\neq}$ = 12 ± 4 e.u.), on the other hand, is greater than for the lighter metals, following the order Fe < Ru < Os. The mechanism of proton transfer and trends in the energetics of the various steps upon changing the nature of the metal atom are discussed.

Introduction

Proton transfer to transition-metal hydrides continues to attract attention[1,2] because of its fundamental importance in many areas, from homogeneous catalysis[3,4] to H_2 biogenesis.[5,6] It results in the formation of cationic dihydride and/or dihydrogen complexes.[7–10] The latter may also be kinetic protonation products giving ultimately the dihydride.[11–15] In the case of half-sandwich cyclopentadienyl metal dihydride complexes the hydride ligands could occupy different coordination sites, being in the *cisoid* (as shown for instance in structure **I** and **II** below) or *transoid* position (structure **IV**) and the specific *cisoid* case results in a possible dichotomy between classical (**II**) dihydride and

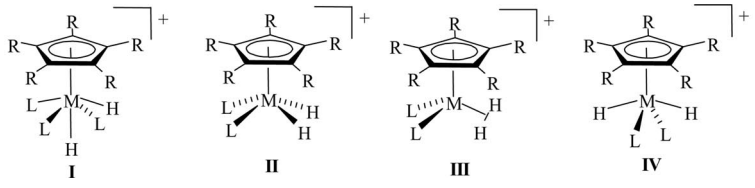

I **II** **III** **IV**

nonclassical (**III**) dihydrogen complexes. Structure **I** was demonstrated for example for compounds $[Cp'Mo(PMe_3)_2LH_2]^+$ (L = CO, Cp′ = Cp*;[16] L = PMe_3, Cp′ = Cp,[17] Cp*[18]), $[CpW(PMe_3)_2(CO)H_2]^+$,[19] and $[CpMo(dppe)(CO)H_2]^+$.[20] For Group 8 complexes of type $[Cp'ML_2H_2]^+$, structure **IV** is typical of all metals (L_2 = 2 PR_3 or bidentate diphosphane),[7,8,12,15,21] whereas structure **II** was only demonstrated spectroscopically at low temperature for a few osmium compounds.[21–23] These structures are usually referred to as *trans* and *cis*; this notation will be used herein as well. The *cis* (**II**) and dihydrogen complex (**III**) could be

[a] A. N. Nesmeyanov Institute of Organoelement Compounds, Russian Academy of Sciences,
28 Vavilov Street, 119991 Moscow, Russian Federation
Fax: +7-499-1355085
E-mail: nataliabelk@ineos.ac.ru
shu@ineos.ac.ru
[b] LCC (Laboratoire de Chimie de Coordination), CNRS, and Université de Toulouse,
205 route de Narbonne, 31077 Toulouse, France
E-mail: rinaldo.poli@lcc-toulouse.fr
[c] Institut Universitaire de France,
103 bd Saint-Michel, 75005 Paris, France

Supporting information for this article is available on the WWW under http://dx.doi.org/10.1002/ejic.200901120.

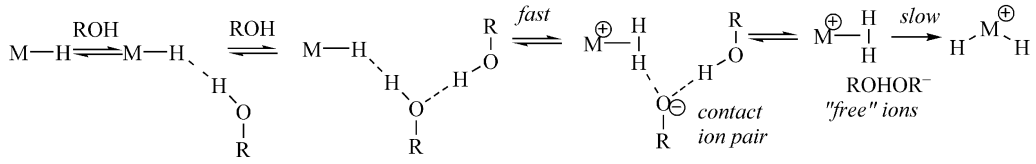

Scheme 1. Mechanism of proton transfer to Cp*MH(dppe) (M = Fe, Ru).

seen as resulting from protonation of the neutral precursors $(C_5R_5)MHL_2$ on the same side (*syn*) as the hydride ligand, whereas the *trans* (**IV**) structure results from proton attack at the opposite side (*anti*).

The metal influence on the properties and relative stability of dihydrogen and dihydride tautomers of Group 8 metal hydrides is known for complexes of several types such as MH_4L_3, $[MH_3L_4]^+$, $[MH_3(PP)_2]^+$, $[MCl(H_2)(PP)_2]^+$, $[MH(H_2)(PP_3)]^+$, and $[CpMH_2(PP)]^+$ [L = phosphanes or monophosphites, CO; PP = chelating phosphanes; PP_3 = $P(CH_2CH_2PR_2)_3$].[24,25] The relative stability of the dihydrogen form decreases when the metal is replaced successively by a heavier metal in the same group. The same trend was found for the (η^2-H_2) ligand acidity. A few exceptions to this general trend have been noted, which could be related to the strong H–H interaction.[24,25] The osmium analogues usually have the least tendency to form dihydrogen complexes. In some cases they give cationic *cis*-dihydride **II** (see structure) upon protonation without the observation of a dihydrogen complex intermediate.[21–23] For example, the result of CpMH(dppe) protonation depends on the metal (Fe, Ru, Os) and temperature. In the case of iron the low-temperature protonation by HBF_4 yields $[CpFe(\eta^2\text{-}H_2)(dppe)]^+$, which remains nonclassical up to room temperature but slowly loses H_2.[14,15] For osmium the same reaction at 198 K yields a mixture of *cis*-$[CpOs(H)_2(dppe)]^+$ and *trans*-$[CpOs(H)_2(dppe)]^+$ in a 1:3 ratio, which changes to 1:70 upon warming to room temperature.[21] Protonation of the ruthenium congener was reported only at room temperature to yield a 1:2 mixture of $[CpRu(\eta^2\text{-}H_2)(dppe)]^+$ and *trans*-$[CpRuH_2(dppe)]^+$.[26]

For the recently studied series of Group 8 Cp*M(dppe)H complexes (M = Fe,[15,27,28] Ru,[29] Os[23]), the low-temperature protonation by strong acids (195 K, CD_2Cl_2) yields (η^2-H_2) (Fe, Ru) or *cis*-$(H)_2$ (Os) complexes as kinetic products of *syn* protonation. For all three metals they convert into the corresponding *trans*-dihydrides upon warming. The use of weak proton donors allowed establishing the following proton-transfer mechanism for M = Fe and Ru (Scheme 1).

After the reversible dihydrogen bond formation the proton transfer occurs with participation of a second proton donor molecule. The irreversible isomerization $[Cp^*M(\eta^2\text{-}H_2)(dppe)]^+ \rightarrow$ *trans*-$[Cp^*M(H)_2(dppe)]^+$ occurs upon ion-pair dissociation. The enthalpy of dihydrogen bond formation and proton transfer increases from iron to ruthenium, whereas the activation parameters for the subsequent isomerization are very similar. The theoretical study of the dihydrogen–dihydride transformation mechanism for M = Fe showed that it involves a ligand reorganization without intermediates.[30] Notably, no stationary point was found corresponding to a putative *cis*-dihydride isomer. The present work aims at shining more light on the mechanism of proton transfer to Cp*Os(dppe)H.

Results

Interaction with Weak Proton Donors: Characterization of the Hydrogen-Bonded Intermediate

In order to investigate the mechanism of the protonation of Cp*OsH(dppe), **1**, in more detail, its interaction with different proton donors was studied by IR (ν_{OH} and ν_{OsH}) and NMR spectroscopy in the 190–300 K temperature range. According to our well-established protocol,[31] the following set of OH and NH proton donors was used: CFH_2CH_2OH (MFE), CF_3CH_2OH (TFE), and $(CF_3)_2$-CHOH (HFIP), indole. In the presence of excess hydride in any solvent used (CH_2Cl_2, alkanes or their mixtures), the IR spectra of MFE and TFE in the ν_{OH} region show a typical picture of hydrogen bond formation. The intensity decrease of the alcohol ν_{OH}^{free} band is accompanied by the appearance of a new broad low frequency ν_{OH}^{bonded} band typical of hydrogen-bonded OH (Table 1).

Table 1. Parameters of the hydrogen bonding between Cp*OsH(dppe) and MFE or TFE in CH_2Cl_2.

ROH	P_i[a]	$\nu_{OH(free)}$ [cm^{-1}]	$\nu_{OH(bonded)}$ [cm^{-1}]	$\Delta\nu$ [cm^{-1}]	ΔH[b] [kcal mol^{-1}]	E_j[c]
MFE	0.74	3614	3338	276	–5.0	1.47
TFE	0.89	3592	3229	363	–6.0	1.47

[a] Acidity factors of proton donors.[35] [b] Calculated by Equation (1), mean error ± 0.4 kcal mol^{-1}. [c] Basicity factor as defined in Equation (2), ΔH_{11} = –4.6 kcal mol^{-1} for CH_2Cl_2.[35]

As expected, the interaction with the more fluorinated alcohol – TFE – is stronger than with MFE, as indicated by the greater band shift $\Delta\nu_{OH} = \nu_{OH}^{free} - \nu_{OH}^{bonded}$. The interaction enthalpies were obtained using Iogansen's empirical correlation [Equation (1)].[32,33] Analysis of the temperature dependence of the H-bond formation constants for TFE gives ΔH = –6.1 kcal mol^{-1} and ΔS = –19.7 e.u. The basicity factor E_j = 1.47 obtained by Equation (2) can be compared with those found for the Ru (1.39)[29] and Fe (1.35)[27] analogues. These data show the expected basicity increase on descending the group, similarly to the PP_3MH_2 hydride series (PP_3 = $P(CH_2CH_2PPh_2)_3$, M = Fe, Ru, Os).[34] However, the E_j range is narrower for the Cp*MH(dppe) series than for the PP_3MH_2 series (1.12–1.67).

$$\Delta H = 18\Delta\nu/(\Delta\nu + 720) \quad (1)$$

$$E_j = \Delta H_{ij}/(\Delta H_{11} P_i) \quad (2)$$

The IR spectrum of **1** in the Os–H stretching vibration region was studied in the presence of proton donors in different solvents. The ν_{MH} band of the hydride complex **1** (2033 cm^{-1}, $\Delta\nu_{1/2}$ = 56 cm^{-1} at 200 K) is quite symmetric as shown in Figure 1 and partially overlaps on the low frequency side with a dppe ligand overtone. Its intensity decreases as the temperature increases (ε = 84 and 63 $L\,mol^{-1}\,cm^{-1}$ at 200 and 250 K, respectively). Titration of **1** by TFE in hexane at 200 K causes the ν_{OsH} band intensity to increase when using up to 4 equiv. of the proton donor. However, no ν_{OsH} band shift was observed under these conditions. Further addition of the proton donor causes an intensity decrease, explained by the proton transfer (see Figure S1). When the same study was carried out in the more polar dichloromethane, only the ν_{OsH} band decrease due to protonation was observed with any amount of proton donor. No low-frequency shifts/shoulders expected for dihydrogen-bonded adducts were revealed. A similar behavior was observed for the Ru analogue in these solvents.[29]

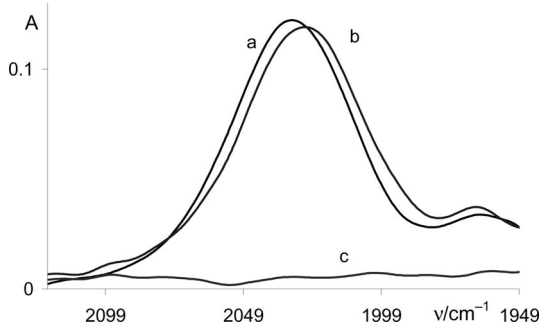

Figure 1. IR spectra (ν_{OsH} region) of Cp*OsH(dppe) (**1**) (0.017 M) (a), **1** in the presence of indole (5 equiv.) (b). Methylcyclopentane/dichloromethane, 2:1 v/v mixture, 190 K. Spectrum of indole (0.085 M) (c) is shown for comparison.

In the case of the Ru system, use of a 2:1 v/v hexane (or methylcyclopentane)/dichloromethane mixture revealed low-frequency ν_{MH} shoulders in the presence of MFE or TFE, evidencing *syn* addition with formation of a dihydrogen-bonded adduct. In the case of osmium, on the other hand, only a band intensity increase and no low-frequency shoulders were observed under these conditions. However, a low-frequency shift (of –5 cm^{-1}) became observable in the presence of the weaker proton donor indole (5 equiv.) (Figure 1), also suggesting *syn* addition of the proton donor for this metal.

The low-temperature NMR study of **1** in the presence of excess TFE in CD_2Cl_2 shows the expected changes for dihydrogen bond formation:[31] the hydride resonance shifts upfield ($\Delta\delta$ = –0.05 and –0.07 with 2.7 and 4.5 equiv. TFE respectively, see Figure S2). The $^{31}P\{^1H\}$ resonance shifts by –0.4 and –0.5 ppm, respectively. The T_{1min} value of the hydride resonance substantially decreases upon proton donor addition, being 270 ms at 230 K (500 MHz) in the presence of 2.7 equiv. of TFE (vs. 850 ms at 220 K for **1**). The presence of *cis*-$[Cp^*Os(H)_2(dppe)]^+$, *cis*-$\mathbf{1H}^+$ (6% and 20% for 2.7 and 4.5 equiv. of TFE), is evident from the appearance of a virtual triplet signal at –13.32 ppm in the ^1H NMR spectrum (having a T_1 of ca. 270 ms at 200 K). Much smaller $\Delta\delta$ values were found for the interaction between **1** and MFE (3 and 7 equiv.): –0.005 and –0.011 for ^1H and –0.03 and –0.06 for $^{31}P\{^1H\}$ (see Figure S3). Both the IR and NMR spectroscopic data obtained for the interaction of Cp*OsH(dppe) with proton donors as well as those obtained earlier for the iron and ruthenium congeners conform to the criteria of M–H···H-A bond formation.[31]

Interaction with *p*-Nitrophenol – Ion Pairing in *cis*-$[Cp^*Os(H)_2(dppe)]^+X^-$

The equilibrium resulting from the interaction between Cp*OsH(dppe) and *p*-nitrophenol (PNP, P_i = 1.27) was investigated with the aim to obtain data about ion pairs formed as the result of proton transfer. Following the approach developed in our laboratories,[28,29,36] UV/Vis spectra were recorded for CH_2Cl_2 solutions of PNP (0.001 M) in the presence of **1** at ratios from 1:0.1 to 1:2 at 200 K. As expected the spectra show wide overlapping bands resulting from various forms of phenol and the hydride complex

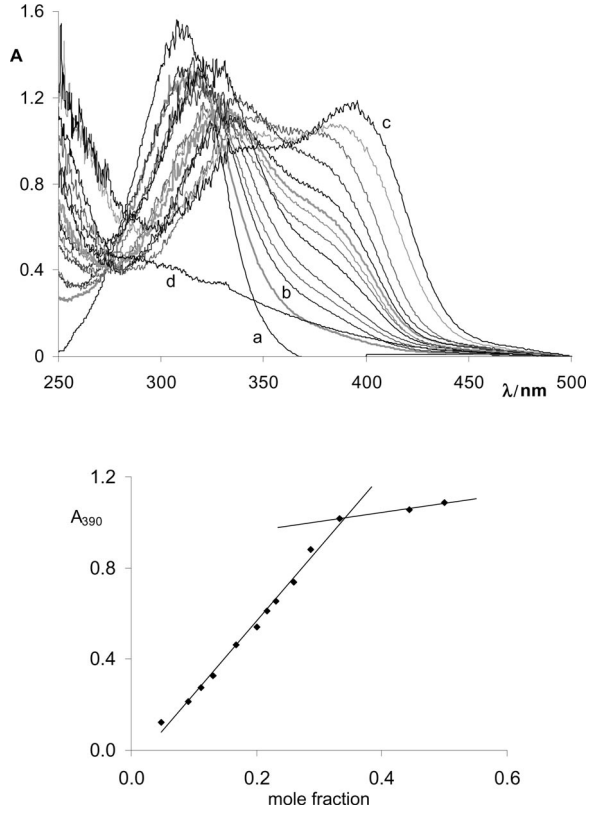

Figure 2. UV/Vis spectra (top) of PNP (0.002 M, a) in the presence of 0.05 (b) to 1.0 (c) equiv. Cp*OsH(dppe) (**1**) and the corresponding titration plot (bottom). CH_2Cl_2, 200 K. Mole fraction = c(**1**)/[c(**1**) + c(PNP)]. The spectrum of **1** (0.0023 M, d) is also given for comparison.

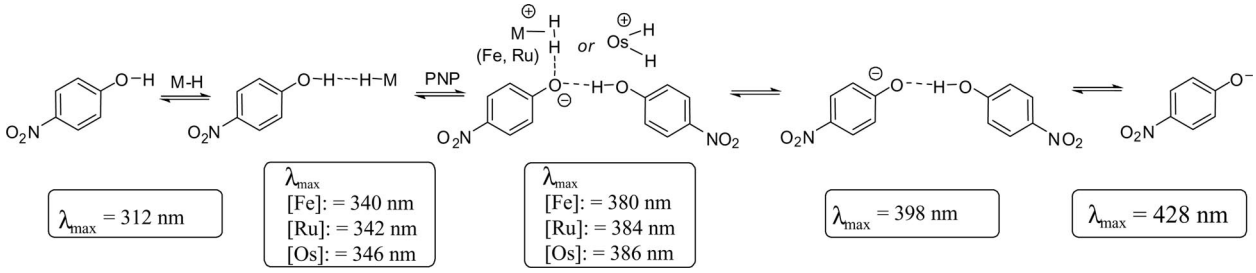

Scheme 2. Summary of UV/Vis absorption frequencies of various forms of PNP and its conjugate anion.

(both free and hydrogen bonded) (Figure 2 and Scheme 2). The absence of free phenolate is signaled by the absence of a band at 430 nm.

Band decomposition yields three bands with maxima at 312, 346, and 386 nm. The first two are assigned to free PNP and to the dihydrogen-bonded complex [Cp*(dppe)-OsH]···$HOC_6H_4NO_2$. The band at 386 nm is attributed to a hydrogen-bonded phenolate ion, since this is blue-shifted from the free ArO-band by 44 nm. The anion appears to be present in the form of a homoconjugate ion on the basis of a titration experiment. Upon increasing the amount of **1** at constant PNP concentration at 200 K, the bands at 346 nm and 386 nm grow in intensity whereas the free phenol band at 312 nm decreases (Figure 2, top). Plotting the intensity at 390 nm vs. the Cp*OsH(dppe) mol fraction (Figure 2, bottom) gives a break point for a mol fraction of 0.33, indicating a 1:2 binding stoichiometry for the ionic species, *cis*-$[Cp^*(dppe)Os(H)_2]^+[ArOHOAr]^-$. The same ion-pair composition was shown previously for the cationic dihydrogen complexes of iron and ruthenium, $[Cp^*(dppe)M(\eta^2\text{-}H_2)]^+$-$[ArOHOAr]^-$. The 14 nm blue-shift of this band relative to free $[ArOHOAr]^-$ suggests[37] further hydrogen bonding of the homoconjugated anion with the cationic dihydrogen complex, $[Cp^*(dppe)OsH_2]^+$···$[ArOHOAr]^-$. Note that on descending the group both bands attributed to the hydrogen-bonded complex and ion pair shift slightly to longer wavelengths; the hydrogen-bonded complex band appears at 340, 342, and 346 nm and that of the ion pair is at 380, 384, and 386 nm for Fe, Ru, and Os, respectively. This is in agreement with an increase of hydride proton accepting ability and weakening of hydrogen bonding within the ion pair on going down the Group.

Protonation by $HBF_4{\cdot}Et_2O$: Characterization of *cis*- and *trans*-$[Cp^*Os(dppe)H_2]^+$

We have shown recently[23] that *cis*-$[Cp^*Os(dppe)H_2]^+$ is the kinetic product (193 K) when protonating **1** with $HBF_4{\cdot}Et_2O$, then irreversibly transforming into the *trans*-isomer upon warming (above 233 K). Both *cis*- and *trans*-**1H**$^+$ were characterized by NMR spectroscopy in CD_2Cl_2. In this contribution, we complete the characterization of these complexes by an IR study and by structural analysis of *trans*-**1H**$^+$$BF_4^-$.

Addition of ca. 1 equiv. $HBF_4{\cdot}Et_2O$ to the solution of **1** in CH_2Cl_2 at 200 K causes the complete disappearance of the Os–H stretching band of **1** (Table 2) and the appearance of two new bands at 2126 and 2177 cm^{-1} belonging to *cis*-**1H**$^+$ in the IR spectrum (Table 2, Figure 3). These two bands were attributed to the symmetric ν^s and asymmetric ν^{as} OsH_2 stretching vibrations on the basis of the theoretical calculations (Table S1). This spectrum remains essentially unchanged so long as the temperature remains below 230 K. At higher temperatures, slow conversion to the *trans*-dihydride complex (*trans*-**1H**$^+$) occurs, eventually yielding two new bands at 2053 and 2102 cm^{-1} (Figure 3, spectrum c).

Table 2. IR spectroscopic parameters of the ν_{MH} and ν_{MH2} bands of Cp*MH(dppe) hydrides and their protonation products, $[Cp^*MH_2(dppe)]^+$, in CH_2Cl_2 at 200 K.

M	Cp*MH(dppe)		*trans*-$[Cp^*M(H)_2(dppe)]^+$			
	ν_{MH} ($\Delta\nu_{1/2}$)[a]	ε[b]	ν^s_{MH2} ($\Delta\nu_{1/2}$)[a]	ε[b]	ν^{as}_{MH2} ($\Delta\nu_{1/2}$)[a]	ε[b]
Fe	1844 (48)	12	1940 (40)	4		
Ru	1918 (58)	34	2002 (56)	14	1968 (26)	8
Os	2033 (56)	83	2102 (40)	41	2053 (24)	25
			2126 (55)[c]	*16*[c]	*2177 (85)*[c]	*29*[c]

[a] In cm^{-1}. [b] Molar absorption coefficient in $L\,mol^{-1}\,cm^{-1}$. [c] *cis*-H_2

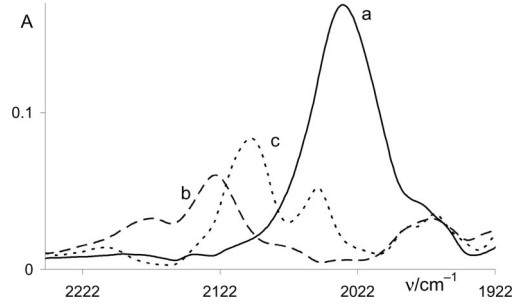

Figure 3. IR spectra (ν_{OsH} region) of Cp*Os(dppe)H (**1**, 0.017 M) (a); *cis*-**1H**$^+$ generated in situ[38] by mixing **1** and ca. 1 equiv. $HBF_4{\cdot}Et_2O$ (b) and *trans*-1H$^+$, obtained from (b) after warming to 298 K and cooling back (c). CH_2Cl_2, 200 K, l = 1.2 mm.

Careful reinvestigation of the previously reported[29] IR spectrum of the *trans*-$[Cp^*Ru(H)_2(dppe)]^+$ complex revealed two ν_{RuH2} bands at 1968 and 2002 cm^{-1} (see Figure S4 and Table 2 and Table S1), whereas only the stronger one was described previously. On the other hand the IR

Table 3. Key bond lengths [Å] and angles [°] for hydride **1** and its protonation products *cis*-**1H**$^+$ and *trans*-**1H**$^+$ according to the single-crystal X-ray data and the DFT B3PW91 calculations on model Cp*OsH(dhpe) (**1$_t$**) and real (**1**) complexes.[a]

		1		*cis*-**1H**$^+$			*trans*-**1H**$^+$	
	X-ray[b]	DFT **1$_t$**	DFT **1**	DFT *cis*-**1$_t$H**$^+$	DFT *cis*-**1H**$^+$	X-ray	DFT *trans*-**1$_t$H**$^+$	DFT *trans*-**1H**$^+$
Os–H	1.56	1.635	1.627	1.615	1.602	1.45(3)	1.638	1.628
				1.619	1.610	1.42(4)	1.641	1.631
Os–CNT	1.90(3)	1.936	1.955	1.952	1.977	1.888(2)	1.931	1.945
Os–P(1)	2.2357(9)	2.253	2.264	2.321	2.345	2.2841(9)	2.315	2.330
Os–P(2)	2.2302(10)	2.252	2.267	2.319	2.371	2.2836(9)	2.310	2.324
∠ H–Os–H				61.3	62.8	133(2)	134.4	132.3
∠ CNT–Os–H	119(3)	122.2	119.8	116.4	111.6	111(2)	112.1	114.6
				119.7	120.0	116(2)	113.5	113.1
∠ CNT–Os–P(1)	134.0(4)	132.4	133.3	126.1	127.5	136.04(5)	136.8	136.9
∠ CNT–Os–P(2)	135(2)	132.7	134.0	127.1	130.3	136.34(5)	136.8	135.1
∠ P(1)–M–P(2)	78.0(2)	83.7	85.2	81.3	81.3	87.11(3)	86.4	87.9

[a] See computational section for details. [b] Data from ref.[29]

spectrum of the *trans*-[Cp*Fe(H)$_2$(dppe)]$^+$ complex features only one band at 1940 cm^{-1}. This can be explained by the lower intensity of the ν^s_{FeH2} band and by the decrease of the difference between ν^s_{MH2} and ν^{as}_{MH2} (Table 2 and Table S1) on ascending the group ($\Delta\nu = \nu^s_{MH2} - \nu^{as}_{MH2}$ = 51 cm^{-1} for Os and 35 cm^{-1} for Ru) leading to band superposition for Fe. Another interesting feature is a decrease of the band shift upon protonation on descending the group. Taken as the difference between the starting hydride ν_{M-H} band and the higher intensity ν_{MH2} band of the *trans*-dihydride, the band shift $\Delta\nu$ = 100, 86, and 71 cm^{-1} for M = Fe, Ru, and Os, respectively.

The molecular structure of *trans*-[Cp*Os(dppe)(H)$_2$]$^+$-BF$_4^-$ was determined by single-crystal X-ray analysis (Figure 4); the main geometrical parameters are collected in Table 3. The two hydrides were located and fully refined with isotropic thermal parameters. The coordination geometry around osmium can be described as a distorted four-legged piano stool. The two hydride atoms are in *transoid* position with an H(1)–Os(1)–H(2) angle much larger than that for *trans*-[Cp*Fe(dppe)(H)$_2$]$^+$BF$_4^-$ (133(3)° vs. 110.5°),[15] whereas the Os–H bonds and Fe–H bonds are identical within the experimental error [1.45(3)–1.42(4) Å vs. 1.48–1.50 Å].[15] Relative to the iron analogue, the P(1)–M–P(2) angle is smaller [87.11(3)° vs. 90.73(8)°], whereas the Os–P and Os–CNT distances are slightly longer [2.2841(9)–2.2836(9) Å and 1.888(2) Å vs. 2.170(2)–2.166(2) Å and 1.728(6) Å].

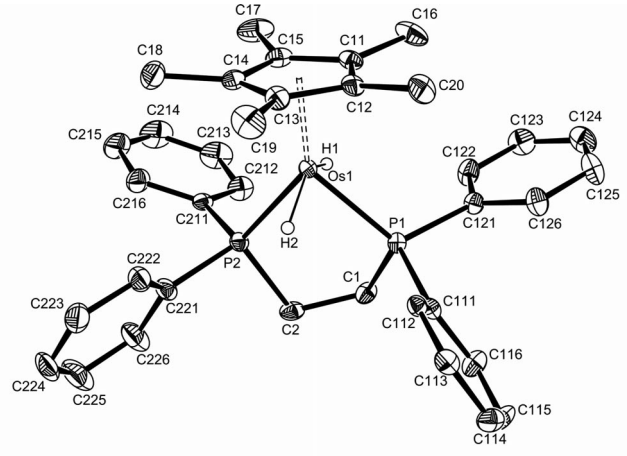

Figure 4. Molecular structure of *trans*-[Cp*Os(dppe)(H)$_2$]$^+$BF$_4^-$ (30% probability level).

Kinetic Study on the "*cis*/*trans*" Isomerization

The previously reported ^{1}H NMR study of the *cis*/*trans* isomerization of **1H**$^+$ was limited to 250 K, giving the rate constant $k = 3.15 \pm 0.02 \times 10^{-4}$ s^{-1}.[23] We have now carried out a variable temperature study in order to obtain the activation parameters.[39] An example of the ^{1}H NMR monitoring study is shown in Figure 5.

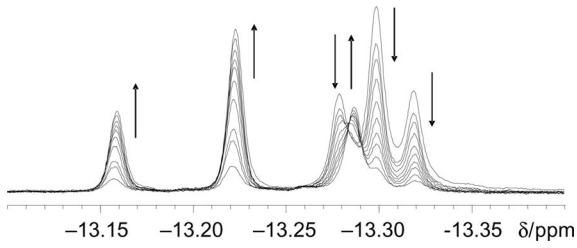

Figure 5. ^{1}H NMR (500 MHz) monitoring (hydride region) of the *cis*-**1H**$^+$ → *trans*-**1H**$^+$ isomerization at 250 K, CD_2Cl_2. *c*(*cis*-**1H**$^+$) = 0.017 M.

The data obtained at each temperature gave an excellent fit to the first-order rate law yielding the isomerization rate constants reported in Figure 6. The Eyring analysis of the rate constants (Figure S5) yields the activation parameters $\Delta H^{\neq} = 21.5 \pm 1.0$ kcal mol^{-1} and $\Delta S^{\neq} = 12 \pm 4$ e.u. The activation enthalpy value is identical, within experimental error, to those found for the iron ($\Delta H^{\neq} = 21.6 \pm 0.8$ kcal mol^{-1})[30] and ruthenium ($\Delta H^{\neq} = 20.9 \pm 0.8$ kcal mol^{-1})[29] M(η^2-H$_2$)$^+$ → *trans*-M(H)$_2^+$ isomerization process, whereas the entropy values tend to increase on descending the group ($\Delta S^{\neq} = 5 \pm 3$ e.u. for Fe and $\Delta S^{\neq} = 9 \pm 3$ e.u. for Ru) resulting in the increase of the isomerization rate constant in the order $k_{Fe} < k_{Ru} < k_{Os}$ at any given temperature.

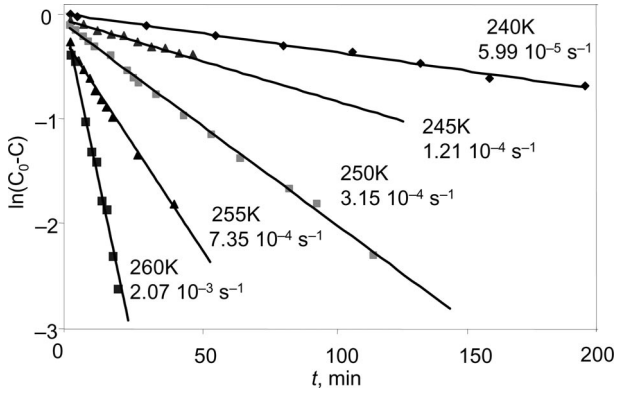

Figure 6. Logarithmic plots of the hydride resonance (–13.17 ppm) appearance for *trans*-$[Cp^*Os(dppe)(H)_2]^+BF_4^-$. Temperatures and the corresponding rate constants are indicated near to the lines.

The isotope effect in the isomerization process was investigated using CF_3SO_3X (X = H, D) at 250 K, yielding the rate constants $k_H = 2.48 \pm 0.05 \times 10^{-4}\ s^{-1}$ and $k_D = 1.86 \pm 0.04 \times 10^{-4}\ s^{-1}$. The kinetic isotope effect k_{HH}/k_{HD} = 1.33 compares to 1.24 previously reported for iron,[30] suggesting a similar intramolecular mechanism for the two isomerization processes. No scrambling of the *cis*-**1D$^+$** compound with *cis*-**1H$^+$** and *cis*-$[Cp^*Os(dppe)(D)_2]^+$ was observed and the isomerization produced *trans*-**1D$^+$** selectively, indicating that the initial protonation process is irreversible and that the isomerization is intramolecular.

Computational Study

The computational analysis of hydrogen bonding and proton transfer was carried out at the DFT/B3PW91 level, using HFIP as the proton donor and the model complex $Cp^*OsH(dhpe)$ (**1_t**), where the phenyl rings of the dppe ligand are replaced by H atoms. A similar study on the Fe analogue was previously reported using either 1 or 2 HFIP molecules, although using a different method (B3LYP) and the simpler CpFeH(dhpe) model.[28] Our study started with the analysis of the H-bonding and proton transfer to the *syn* site. The optimized geometries of the hydrogen-bonded complexes $Cp^*(dhpe)OsH\cdots(HFIP)_x$ (x = 1, 2) and of the proton-transfer product, *cis*-**1_tH^+**$\cdots[(CF_3)_2CHO\cdots H\cdots OCH(CF_3)_2]^-$, are depicted in Figure 7.

As expected the formation of *syn*-**1_t**·HFIP entails the lengthening of the O–H and Os–H bonds relative to the isolated compounds by Δr(OH) = 0.024 Å and Δr(Os–H) = 0.006 Å. The (Os)H···H(O) distance is quite short, but the overall geometry of the Os–H···HO fragment (Os···H distance 2.924 Å, ∠Os···H–O = 158°, ∠H···H–O = 152°) indicates an asymmetric bifurcated interaction with a contri-

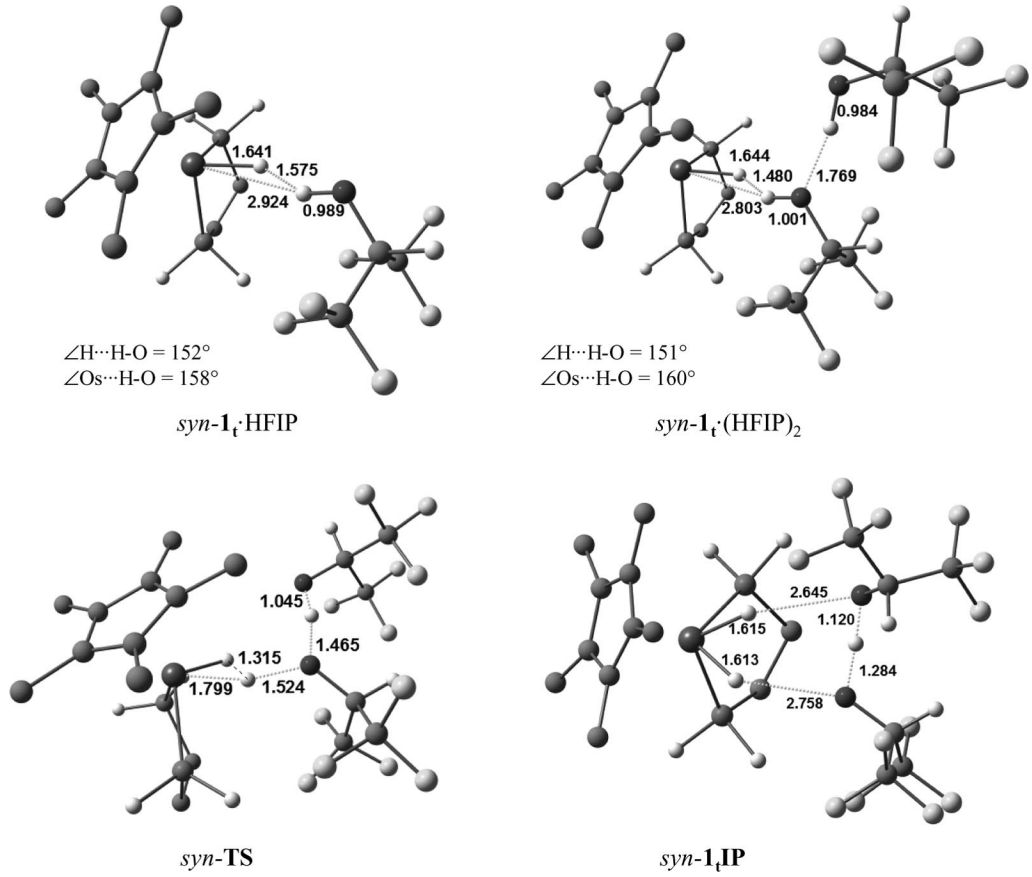

Figure 7. Optimized geometries of the hydrogen bonded, transition state, and final ion-pair complexes related to the *syn* proton donor addition to **1_t**, with selected bond lengths in Å. Hydrogen atoms of the Cp* ligand and of the ethylene backbone are removed for clarity.

bution from the metal atom. Similar structural features were found for the hydrogen-bonded adducts of complex $Cp^*WH_3(dppe)$.[40] The Os···H(O) and (Os)H···H(O) distances shorten while the Os–H and O–H bonds elongate upon binding of the second alcohol molecule in agreement with stronger binding in the *syn*-$\mathbf{1_t}$·$(HFIP)_2$ adduct. The minimum for the *syn*-$\mathbf{1_t}$·HFIP adduct is found 10.7 kcal mol^{-1} below the isolated reactants, whereas addition of the second alcohol molecule brings it further down to –21.3 kcal mol^{-1}. The formation energy of the latter complex considerably exceeds the sum of the formation energies for the $\mathbf{1_t}$·HFIP adduct and the HFIP dimer (–7.5 kcal mol^{-1}) due to a cooperative effect, which was calculated as ΔE_{coop} = ΔE[$\mathbf{1_t}$·$(HFIP)_2$] – ΔE($\mathbf{1_t}$·HFIP) – ΔE[$(HFIP)_2$] = –4.5 kcal mol^{-1}. As expected,[41] consideration of the solvent by means of single-point CPCM calculations lowers all the formation energies, the *syn*-$\mathbf{1_t}$·$(HFIP)_2$ adduct being found only –3.5 kcal mol^{-1} below the reactants in CH_2Cl_2 (see the energy profile in Figure S6).

Proton transfer was only investigated starting from the 1:2 adduct, *syn*-$\mathbf{1_t}$·$(HFIP)_2$, because when using only one HFIP molecule the proton-transfer product did not afford a local minimum and reverted back to the H-bonded adduct, like for the previously published Fe system.[28] The proton-transfer transition state, *syn*-**TS** (Figure 7), features an almost fully formed Os–H bond, with a distance between the hydride ligand and the incoming proton (1.315 Å) far above that typical of (η^2-H_2) complexes. The most stable configuration of the *cis*-$\mathbf{1_tH^+}$···[$(CF_3)_2$CHO···H···OCH-$(CF_3)_2$]$^-$ ion pair (*syn*-$\mathbf{1_t}$**IP**) features a quite symmetrical cation–anion arrangement with two (Os)H···O hydrogen bonds (Figure 7). The distance between the two hydride ligands is 1.552 Å. Thus, formation of the *cis*-dihydride complex occurs via the direct *syn* protonation of the metal atom assisted by the interaction with the hydride ligand. No minimum for an (η2-H_2) complex could be found. The transition state *syn*-**TS** is above *syn*-$\mathbf{1_t}$·$(HFIP)_2$ by 13.8 kcal mol^{-1} in the gas phase and 10.2 kcal mol^{-1} in dichloromethane. The product ion pair is 4.0 kcal mol^{-1} higher than the *syn*-$\mathbf{1_t}$·$(HFIP)_2$ adduct in the gas phase and 0.5 kcal mol^{-1} lower in dichloromethane. Thus, the *syn* proton transfer is rendered favorable by the solvent effect in CH_2Cl_2. The full energetic profile for hydrogen bonding and proton transfer in the gas phase and in CH_2Cl_2 solution is available in the Supporting Information (Figure S6).

The *anti* addition has only been studied for the more favorable 1:2 adduct, *anti*-$\mathbf{1_t}$·$(HFIP)_2$. As already found for the Fe analogue,[28] this hydrogen-bonded adduct is less energetically favorable than the corresponding *syn*-$\mathbf{1_t}$·$(HFIP)_2$. Its optimized geometry is shown in Figure 8 and its relative energy is included in Figure S6. The most relevant structural change is the shortening of the Os–H distance [Δr(Os–H) = –0.006 Å]. The *anti* protonation to yield *trans*-$\mathbf{1_tH^+}$···[R^FO···H···OR^F]$^-$ features a transition state, *anti*-**TS** at 6.7 kcal mol^{-1} (in the gas phase) and 4.8 kcal mol^{-1} (in dichloromethane) above the corresponding metal-bound hydrogen-bonded adduct, *anti*-$\mathbf{1_t}$·$(HFIP)_2$. Since the energetically preferred adduct is the dihydrogen-bonded complex *syn*-$\mathbf{1_t}$·$(HFIP)_2$, the latter can be regarded as the system "resting state." Hence, the proton-transfer barrier becomes almost identical for the two pathways in dichloromethane (Figure S6).

For comparison, the two protonation pathways for the iron analogue were reinvestigated using the same computational level (B3PW91) and model [Cp*FeH(dhpe)] ($\mathbf{2_t}$) as for the Os system. The complete energy profiles for hydrogen bond formation and proton transfer, for both *syn* and *anti* additions, are provided in the Supporting Information (Figure S7). In spite of the lower E_j, $\mathbf{2_t}$ gave slightly greater formation energies for the more stable *syn*-$\mathbf{2_t}$·$(HFIP)_2$ adduct (Figure 9), –22.4 kcal mol^{-1} in the gas phase and –4.2 kcal mol^{-1} in CH_2Cl_2 relative to the isolated reactants, than the osmium analogue. The transition state for the *syn* protonation to yield the nonclassical kinetic protonation product, [Cp*Fe(η^2-H_2)(dhpe)]$^+$···[R^FO···H···OR^F]$^-$, *syn*-$\mathbf{2^tIP}$, is above $\mathbf{2_t}$·$(HFIP)_2$ by 7.6 kcal mol^{-1} in the gas phase and by 4.9 kcal mol^{-1} in dichloromethane, both being ca. half those of the related osmium system. On the other hand, the *anti* protonation to yield *trans*-$\mathbf{2_tH^+}$···[R^FO···H···OR^F]$^-$, *anti*-$\mathbf{2^tIP}$, is characterized by a higher activation barrier, reaching 12.3 kcal mol^{-1} in the gas phase and 9.7 kcal mol^{-1} in dichloromethane relative to the corresponding *anti*-$\mathbf{2_t}$·$(HFIP)_2$ local minimum (Figure S7), which corresponds to 20.2 kcal mol^{-1} and 18.0 kcal mol^{-1},

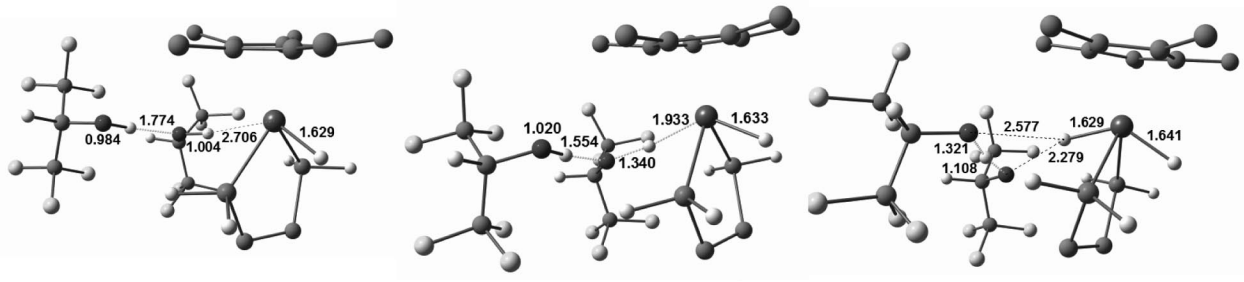

anti-$\mathbf{1_t}$·$(HFIP)_2$ *anti*-**TS** *anti*-$\mathbf{1_t}$**IP**

Figure 8. Optimized geometries of the hydrogen bonded, transition state, and final ion-pair complexes related to the *anti* proton donor addition to $\mathbf{1_t}$, with selected bond lengths in Å. Hydrogen atoms of the Cp* ligand and of the ethylene backbone are removed for clarity.

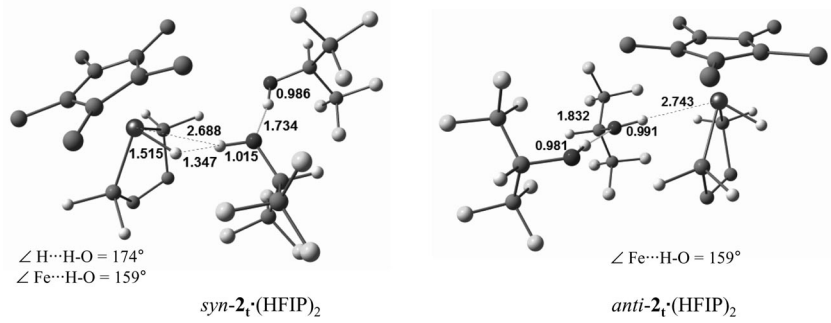

Figure 9. Optimized geometries of the hydrogen-bonded complexes between Cp*FeH(dhpe) ($\mathbf{2_t}$) and two HFIP molecules, with selected bond lengths in Å. Hydrogen atoms of the Cp* ligand and of the ethylene backbone are removed for clarity.

respectively, from the "resting state" *syn*-$\mathbf{2_t}$·$(HFIP)_2$ (Figure S7).

The last point addressed by the computational study is the *cis*/*trans* isomerization mechanism for $\mathbf{1H^+}$. This study was carried out on both the model $[Cp^*OsH_2(dhpe)]^+$ ($\mathbf{1_tH^+}$) and the full $[Cp^*OsH_2(dppe)]^+$ system, without consideration of the counterion. The optimized geometries of the model and full *trans* systems are in close correspondence with the experimentally observed structure (Table 3), the only major discrepancy being the Os–H distances which are notoriously underestimated in X-ray structural determinations. It is also notable that the experimental bond lengths are better matched by the model system, although the discrepancy between model and full systems is small. The bond angles are quite close to the experimental values]– for both systems. For comparison, the calculations were also carried out for the neutral precursor **1** (and for the model $\mathbf{1_t}$), and compared with those of the previously reported[23] X-ray structure in Table 3.

The model cation $\mathbf{1_tH^+}$ gives nearly the same gas-phase energy (E^g) for the two isomers (just 0.8 kcal mol^{-1} in favor of *cis*-$\mathbf{1_tH^+}$), but the *trans* isomer becomes preferred by 6 kcal mol^{-1} for the full system $\mathbf{1H^+}$, in agreement with the essentially quantitative isomerization. For comparison, the energy difference between the *syn* and *anti* protonation products for the Ru and Fe systems, $[Cp^*M(\eta^2\text{-}H_2)(dppe)]^+$ and *trans*-$[Cp^*M(dppe)(H)_2]^+$, is 4.9 kcal mol^{-1} and 3.1 kcal mol^{-1}, respectively, in favor of the *anti* isomer. The optimized geometries of these four complexes, reported here for the first time, are available in the SI. The proton affinity of these hydrides, calculated as $-\Delta H$(298 K) for the kinetically controlled *syn* protonation reactions (3) and (4), is 258.6 kcal mol^{-1} for Fe, 257.3 kcal mol^{-1} for Ru, and 263.4 kcal mol^{-1} for Os, placing the basicity of the Os complex higher than that of the Fe and Ru analogues in agreement with the experiment.[42]

$$[Cp^*M(dppe)H] + H^+ \rightarrow [Cp^*M(\eta^2\text{-}H_2)(dppe)]^+ \quad (3)$$

$$[Cp^*Os(dppe)H] + H^+ \rightarrow \textit{cis}\text{-}[Cp^*Os(dppe)(H)_2]^+ \quad (4)$$

The transition state for the *cis*/*trans* isomerization of $\mathbf{1_tH^+}$ displays a similar geometry to that previously reported for the related nonclassical complex of iron (Figure S8) and is located at 25.5 kcal mol^{-1} above *cis*-$\mathbf{1_tH^+}$ in the gas phase (25.1 kcal mol^{-1} in dichloromethane).[30] The isomerization proceeds in a single step by migration of one hydride ligand from one side to the other of the metal coordination sphere with concomitant tilt of the phosphane ligands. The isomerization barrier is slightly lower than that reported for the $[Cp^*Fe(\eta^2\text{-}H_2)(dhpe)]^+$ isomerization in the gas phase (28.9 kcal mol^{-1}).[30] This is in agreement with the slow rate measured experimentally for the osmium system (see above), similar to that of the corresponding Fe system.[30]

Discussion

The overall process of proton transfer to Cp*OsH(dppe) (**1**) can be rationalized as shown in Scheme 3. It parallels the mechanism established for the protonation of the Cp*MH(dppe) complexes of Fe and Ru (Scheme 1), with a kinetically controlled *syn* addition followed by slow isomerization to the thermodynamically more stable *trans* isomer, which corresponds to the expected product of *anti* addition.

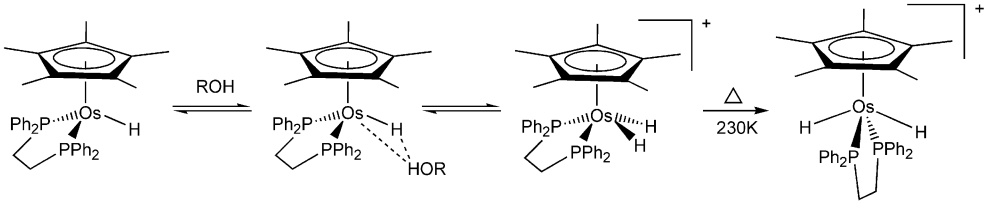

Scheme 3. Proposed mechanism of interaction between **1** and ROH proton donors.

The first step for all three metals is formation of a hydrogen-bonded adduct with two proton donor molecules, since a 1:1 adduct does not have sufficient thermodynamic drive to complete the proton-transfer step. Also common to the three metals is the site preference, the *syn* adduct being more stable than direct bonding to the metal site opposite to the hydride ligand. The hydride basicity in hydrogen bonding (E_j) increases on going down the group in agreement with expectations based on previous studies on other compound families (see Introduction). However, the range is narrower (1.35–1.47 on going from Fe to Os) than for the only other investigated family of Group 8 hydride complexes, PP_3MH_2 (1.12–1.67).[34]

A striking difference between the PP_3MH_2 and Cp*MH(dppe) families is that dihydrogen bonding always leads to a nonclassical (dihydrogen complex) product for the former, whereas a change occurs in the latter: a nonclassical product for Fe and Ru, and a classical *cis* dihydride for Os. The geometrical analysis of the dihydrogen-bonded adducts reveals an asymmetric bifurcated structure with the increasing impact of the M···HO interaction on going from iron to osmium (see Scheme 4). Consequently, the increasing importance of the direct metal participation in hydrogen bonding for the osmium system leads the proton transfer toward the direct formation of the classical *cis*-**1H**$^+$, without involvement of a nonclassical intermediate. Despite its classical nature, *cis*-**1H**$^+$ exists as an ion pair stabilized by hydrogen bonding with the homoconjugated $[R^FO\cdots H\cdots OR^F]^-$ anion similarly to the $[Cp^*(dppe)M(\eta^2\text{-}H_2)]^+$-$[R^FO\cdots H\cdots OR^F]^-$ ion pairs of Fe[28] and Ru.[29]

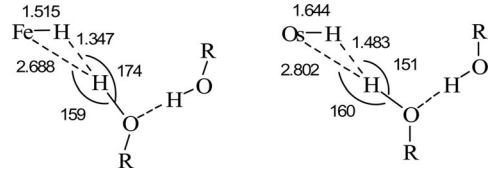

Scheme 4. Comparison of H-bonding parameters for *syn*-Cp*MH(dhpe)·$(HFIP)_2$ with M = Fe and Os.

A similar trend had been previously reported for the $[Cp^*MH_3(dppe)]$ (M = Mo, W) pair of compounds.[40] Although in neither case could a nonclassical intermediate of kinetically controlled protonation at a hydride site be experimentally observed,[40,43] calculations on the simplified $[CpMH_3(dhpe)]$ models revealed a distinct local minimum for a dihydrogen complex $[CpMH_2(H_2)(dhpe)]^+$ in the molybdenum case but none along the proton-transfer pathway for the tungsten system.[40] The maximum energy point for the preferred protonation pathway in the $[Cp^*WH_3(dppe)]$ system has a dihydrogen character, with a H···H distance of 1.102 Å.[40] For the presently investigated [Cp*OsH(dhpe)] complex, on the other hand, the H···H distance is much longer (1.315 Å in *syn*-**TS**, see Figure 7). On the basis of these distances, it is arguable that assistance by the hydride ligand for the direct proton transfer to the metal is greater for $CpWH_3(dppe)$[40] than for compound **1**.

It is interesting to understand what factors orient the proton transfer directly toward the metal (with a greater or smaller assistance by a hydride ligand) to form a classical product, or produce a well-defined nonclassical local minimum. Whenever lone pairs are available on the metal site, they can compete with the high-energy electrons in the M–H bond(s) as hydrogen bonding sites and the resulting interaction may have a component from both types of electron density (bifurcation). For the same structural type, it seems clear from the results obtained so far that the electron density increase associated with a change of metal from the lighter to the heavier member of the same group increases the aptitude of the metal lone pairs to serve as proton acceptors to a greater extent relative to the M–H bonding electrons. However, the details of the coordination sphere also play an important role for systems based on the same metal, as shown by proton transfer to the metal for **1** and to the hydride site for $OsH_2(PP_3)$.

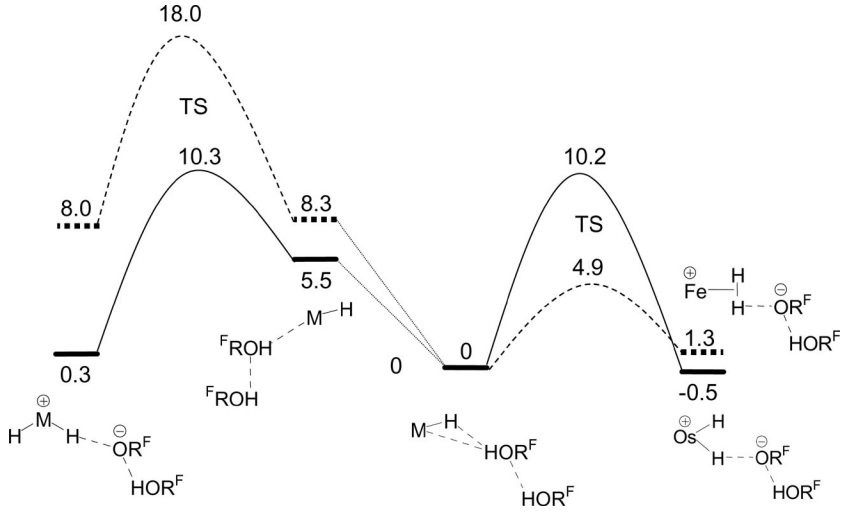

Figure 10. Energy profiles for *syn* (right) and *anti* (left) proton transfer to Cp*MH(dhpe) in dichloromethane (Os: solid lines, Fe: dashed lines). Energies (kcal mol^{-1}) are relative to the "resting state," *syn*-Cp*MH(dhpe)·$(HFIP)_2$.

For the specific Cp*MH(dppe) family, comparison of the two barriers for the *syn* and *anti* protonations, the second one leading directly to the *trans* protonation product, leads to interesting considerations. The calculated barriers relative to the "resting state" *syn*-[Cp*MH(dhpe)]·$(HFIP)_2$ for the Fe and Os systems in dichloromethane solution are compared in Figure 10. The relative energies of the isomeric protonation products shown by these calculations are incorrect (the *trans* product is more stable in the real system) but correct trends were obtained by running calculations on the full system, as shown above in the Results section. The interesting comparisons concern the barriers toward *syn* and *anti* protonation for the same metal (*syn* much faster than *anti* for the Fe system; similar barriers for the Os system), and the barriers for the same type of process (*syn* or *anti*) as the metal changes from Fe to Os (*syn*: faster for Fe than for Os; *anti*: slower for Fe than for Os). The *anti* pathway is easier to analyze because it gives the same product for both metals, whereas the *syn* pathway gives a classical dihydride product for Os and a dihydrogen complex for Fe. For the *anti* protonation, a lower barrier of the Os system is easily rationalized by invoking the greater metal basicity and the more diffuse character of the metal lone pairs, yielding greater thermodynamic stability to the protonation product and a more product-like character to the transition state. In both cases, the metal changes formal oxidation state from II to IV during the process. For the *syn* attack, on the other hand, the Fe complex protonation yields a nonclassical product with little involvement of the metal lone pair at the transition-state level and the metal formal oxidation state remains II throughout the process. The low metal rehybridization required for this process leads to a very low activation barrier. *Syn* protonation of the osmium system leads instead to a classical product with a change of formal oxidation state and a metal rehybridization, entailing a reaction barrier similar to that of the *anti* pathway. It is important to recollect that, although the sterically encumbered complex **1** shows a kinetically preferred *syn* protonation pathway leading to *cis*-$\mathbf{1H}^+$, less sterically encumbered complexes of the same family yield a mixture of *cis* and *trans* isomers under kinetically controlled conditions,[21,22] in agreement with similar barriers for the protonation of both sites.

Conclusions

This work has revealed a large metal atom participation in the "dihydrogen bonding" to Cp*OsH(dppe) and has confirmed that direct proton transfer to a metal lone pair may be a favored process in the presence of a hydride ligand, although the latter provides assistance to this process. In this case the proton approaches the metal along a trajectory featuring a fleeting proton–hydride contact. As a result, the classical dihydride complex *cis*-[Cp*(dppe)Os$(H)_2]^+$ is formed at low temperatures. Its fate, however, is similar to that of lighter nonclassical congeners, the $[Cp^*(dppe)M(\eta^2\text{-}H_2)]^+$ complexes of iron and ruthenium, with transformation into the thermodynamically more stable *trans*-$[Cp^*(dppe)M(H)_2]^+$.

Experimental Section

General: Hydride **1** was prepared as described previously.[23] All samples were prepared under dry argon using standard Schlenk techniques. The solvents used were purified by refluxing over Na (hexane, methylcyclohexane) or CaH_2 (CH_2Cl_2) and distilled prior to use under dry argon. The NMR solvents (Aldrich) were degassed by three freeze-pump-thaw cycles, and then vacuum transferred at room temperature.

The IR measurements were performed with an Infralum 801 FT-IR spectrometer using CaF_2 cells of 0.04–0.22 cm path length. The UV measurements were performed with Specord M-40 and Varian Cary 50 spectrometers. Low-temperature measurements were carried out using a Carl Zeiss (Jena) cryostat under a stream of liquid nitrogen. The accuracy of the experimental temperature adjustment was ±1 K. The cryostat modification allows operation under an inert atmosphere and transfer of reagents (premixed either at low or at room temperature) directly into the cell which is precooled to the required temperature.

The ^1H and $^{31}P\{^1H\}$ data were collected with a Bruker AV500 spectrometer, operating at 500.3 MHz and 202.5 MHz, respectively. The temperature was calibrated with a methanol chemical shift thermometer; the accuracy and stability was ±1 K. All samples were allowed to equilibrate at every temperature for at least 3 min. The spectra were calibrated with the residual solvent resonance (^1H) and with external 85% H_3PO_4 (^{31}P). The conventional inversion-recovery method ($180 - \tau - 90$) was used to determine the variable-temperature longitudinal relaxation time T_1. Standard Bruker software was used for the calculation of the longitudinal relaxation time.

Crystallographic Study: *trans*-$[Cp^*Os(dppe)(H)_2]^+BF_4^-$ was crystallized from dichloromethane by slow evaporation. A single crystal was mounted under inert perfluoropolyether at the tip of a glass fiber and cooled in the cryostream of a Bruker APEX2 CCD diffractometer. Data were collected using monochromatic Mo-K_α radiation (λ = 0.71073). The structure was solved by direct methods (SIR97)[44] and refined by least-squares procedures on F^2 using SHELXL-97.[45] All H atoms attached to carbon were introduced in the calculations in idealized positions and treated as riding models. The absolute structure was determined by refining Flack's parameter.[46] The drawing of the molecules was realized with the help of ORTEP32.[47] Crystal data and refinement parameters are shown in Table 4.

CCDC-754974 contains the supplementary crystallographic data for this paper. These data can be obtained free of charge from The Cambridge Crystallographic Data Centre via www.ccdc.cam.ac.uk/data_request/cif.

Computational Details: Calculations were performed with the Gaussian03[48] package at the DFT/B3PW91 level.[49–51] Effective core potentials (ECP) were used to represent the innermost electrons of the osmium, ruthenium, and iron atoms as well as the electron core of the phosphorus atoms.[52,53] The basis set for the Os, Ru, Fe, and P atoms was that associated with the pseudopotential,[52,53] with a standard double-ζ LANL2DZ contraction, supplemented in the case of P with a set of d-polarization functions.[54] The carbon and hydrogen atoms of the Cp* and dhpe ligands together with the atoms of the proton donor molecules (C, F, H) that are not involved in hydrogen bonds were described with a 6-31G

Table 4. Crystal data and structure refinement parameters for *trans*-$[Cp^*Os(dppe)(H)_2]^+BF_4^-$.

Empirical formula	$C_{36}H_{41}OsP_2BF_4$
Formula weight	812.64
Temperature [K]	180(2)
Wavelength [Å]	0.71073
Crystal system	monoclinic
Space group	P2(1)
a [Å]	11.0513(7)
b [Å]	13.8528(8)
c [Å]	11.9523(7)
α [°]	90
β [°]	113.272(3)
γ [°]	90
Volume [Å^3]	1680.92(17)
Z	2
D (calcd.) [Mg/m^3]	1.606
Abs. coeff. [mm^{-1}]	3.935
F(000)	808
Crystal size [mm]	$0.123 \times 0.099 \times 0.079$
Theta range [°]	2.49–29.20
Reflections collected	45979
Unique reflections [*R*(int)]	8865 [0.0439]
Completeness [%]	99.7
Absorption correction	multiscan
Max./min. transmission	1.0/0.788
Refinement method	F^2
Data/restr./parameters	8865/1/410
Goodness-of-fit on F^2	0.978
R, wR_2 [$I > 2\sigma(I)$]	0.0263, 0.0395
R, wR_2 (all data)	0.0367, 0.0415
Resid. density [e Å^{-3}]	0.733/–0.528
Absolute structure	–0.005(4)

basis set.[55] The phenyl substituents in the case of the dppe ligand were also described with the 6-31G basis set. The hydridic hydrogen atom and the hydrogen and oxygen atoms of the proton donor molecules involved in hydrogen bonding were described with a 6-31G(d,p) set of basis functions.[56]

The structures of the reactants, intermediates, transition states, and products were fully optimized without any symmetry restriction. Transition states were identified by having one imaginary frequency in the Hessian matrix. Intrinsic reaction coordinate (IRC) calculations were carried out in both directions starting from the located transition states. No scaling factor was applied to the calculated frequencies since the optimization was run in the gas phase and the IR spectra were measured in solution.

Solvent effects were taken into account by using the CPCM continuum representation of the solvent,[57,58] using standard options.[48] The solvation free energies were computed in dichloromethane (ε = 8.93) using the gas-phase optimized geometries.

Supporting Information (see also the footnote on the first page of this article): IR and NMR spectra, ν_{MH} and ν_{MH2} frequencies calculated and *xyz* coordinates of all optimized structures.

Acknowledgments

Support by the Russian Foundation for Basic Research (RFBR, project 08-03-00464) and the Division of Chemistry and Material Sciences of Russian Academy of Sciences is gratefully acknowledged. We also thank the Centre National de la Recherche Scientifique (CNRS) and the RFBR for support through a France-Russia bilateral PICS grant, which is continuing within the framework of a GDRE (groupe de recherche européen). O. A. F. thanks the Russian Federation President grant (MK-380.2008.3) for individual support and R. P. thanks the Centre Interuniversitaire de Calcul de Toulouse (CICT, project CALMIP) for granting free computational time.

[1] M. Besora, A. Lledos, F. Maseras, *Chem. Soc. Rev.* **2009**, *38*, 957–966.
[2] G. J. Kubas, *Chem. Rev.* **2007**, *107*, 4152–4205.
[3] C. Bianchini, M. Peruzzini, in: *Recent Advances in Hydride Chemistry* (Eds.: R. Poli, M. Peruzzini), Elsevier Science, Amsterdam, **2001**, pp. 271–297.
[4] L. A. Oro, E. Sola, in: *Recent Advances in Hydride Chemistry* (Eds.: R. Poli, M. Peruzzini), Elsevier Science, Amsterdam, **2001**, pp. 299–327.
[5] R. A. Henderson, in: *Recent Advances in Hydride Chemistry* (Eds.: R. Poli, M. Peruzzini), Elsevier Science, Amsterdam, **2001**, pp. 419–461.
[6] J. F. Capon, F. Gloaguen, F. Y. Petillon, P. Schollhammer, J. Talarmin, *Eur. J. Inorg. Chem.* **2008**, 4671–4681.
[7] P. G. Jessop, R. H. Morris, *Coord. Chem. Rev.* **1992**, *121*, 155–284.
[8] D. M. Heinekey, W. J. Oldham Jr., *Chem. Rev.* **1993**, *93*, 913–926.
[9] G. J. Kubas, *Metal Dihydrogen and σ-Bond Complexes*, Kluwer Academic/Plenum Press, New York, **2001**.
[10] N. K. Szymczak, D. R. Tyler, *Coord. Chem. Rev.* **2008**, *252*, 212–230.
[11] G. Parkin, J. E. Bercaw, *J. Chem. Soc., Chem. Commun.* **1989**, 255–257.
[12] M. S. Chinn, D. M. Heinekey, *J. Am. Chem. Soc.* **1990**, *112*, 5166–5175.
[13] G. Jia, A. J. Lough, R. H. Morris, *Organometallics* **1992**, *11*, 161–171.
[14] P. Hamon, L. Toupet, J.-R. Hamon, C. Lapinte, *Organometallics* **1992**, *11*, 1429–1431.
[15] J. R. Hamon, P. Hamon, L. Toupet, K. Costuas, J. Y. Saillard, *C. R. Chim.* **2002**, *5*, 89–98.
[16] P. A. Dub, N. V. Belkova, O. A. Filippov, J.-C. Daran, L. M. Epstein, A. Lledós, E. S. Shubina, R. Poli, *Chem. Eur. J.* **2010**, *16*, 189–201.
[17] J. C. Fettinger, H.-B. Kraatz, R. Poli, E. A. Quadrelli, R. C. Torralba, *Organometallics* **1998**, *17*, 5767–5775.
[18] M. Baya, P. A. Dub, J. Houghton, J.-C. Daran, R. Poli, N. V. Belkova, E. S. Shubina, L. M. Epstein, A. Lledós, *Inorg. Chem.* **2009**, *48*, 209–220.
[19] M. L. H. Green, A. K. Hughes, P. Lincoln, J. J. Martin-Polo, P. Mountford, A. Sella, L.-L. Wong, J. A. Bandy, T. W. Banks, K. Prout, D. J. Watkin, *J. Chem. Soc., Dalton Trans.* **1992**, 2063–2069.
[20] T.-Y. Cheng, D. J. Szalda, J. Zhang, R. M. Bullock, *Inorg. Chem.* **2006**, *45*, 4712–4720.
[21] G. Jia, W. S. Ng, J. Yao, C.-P. Lau, Y. Chen, *Organometallics* **1996**, *15*, 5039–5045.
[22] J. D. Egbert, R. M. Bullock, D. M. Heinekey, *Organometallics* **2007**, *26*, 2291–2295.
[23] P. A. Dub, N. V. Belkova, K. A. Lyssenko, G. A. Silantyev, L. M. Epstein, E. S. Shubina, J.-C. Daran, R. Poli, *Organometallics* **2008**, *27*, 3307–3311.
[24] G. C. Jia, C. P. Lau, *Coord. Chem. Rev.* **1999**, *192*, 83–108.
[25] R. H. Morris, *Coord. Chem. Rev.* **2008**, *252*, 2381–2394.
[26] F. M. Conroy-Lewis, S. J. Simpson, *J. Chem. Soc., Chem. Commun.* **1987**, 1675–1676.
[27] N. V. Belkova, P. O. Revin, L. M. Epstein, E. V. Vorontsov, V. I. Bakhmutov, E. S. Shubina, E. Collange, R. Poli, *J. Am. Chem. Soc.* **2003**, *125*, 11106–11115.
[28] N. V. Belkova, E. Collange, P. Dub, L. M. Epstein, D. A. Lemenovskii, A. Lledós, O. Maresca, F. Maseras, R. Poli, P. O.

Revin, E. S. Shubina, E. V. Vorontsov, *Chem. Eur. J.* **2005**, *11*, 873–888.

[29] N. V. Belkova, P. A. Dub, M. Baya, J. Houghton, *Inorg. Chim. Acta* **2007**, *360*, 149–162.

[30] M. Baya, O. Maresca, R. Poli, Y. Coppel, F. Maseras, A. Lledós, N. V. Belkova, P. A. Dub, L. M. Epstein, E. S. Shubina, *Inorg. Chem.* **2006**, *45*, 10248–10262.

[31] L. M. Epstein, N. V. Belkova, E. S. Shubina, in: *Recent Advances in Hydride Chemistry* (Eds.: M. Peruzzini, R. Poli), Elsevier, Amsterdam, **2001**, pp. 391–418

[32] A. V. Iogansen, *Theor. Experim. Khim.* **1971**, *7*, 312–317.

[33] A. V. Iogansen, *Spectrochim. Acta Part A* **1999**, *55*, 1585–1612.

[34] E. Gutsul, N. Belkova, M. Sverdlov, L. Epstein, E. Shubina, V. Bakhmutov, T. Gribanova, R. Minyaev, C. Bianchini, M. Peruzzini, F. Zanobini, *Chem. Eur. J.* **2003**, *9*, 2219–2228.

[35] A. V. Iogansen, *Theor. Experim. Khim.* **1971**, *7*, 302–311.

[36] E. Gutsul, N. Belkova, G. Babakhina, L. Epstein, E. Shubina, C. Bianchini, M. Peruzzini, F. Zanobini, *Russ. Chem. Bull.* **2003**, *52*, 1204–1206.

[37] For the parameters of the UV/Vis bands of the free and homoconjugated PNP anion (the latter obtained by mixing equimolar amounts of PNP and potassium *p*-nitrophenolate in the presence of excess 18-crown-6), see ref.[28]

[38] An amount (ca. 8%) of *trans*-[Cp*Os(dppe)H_2]$^+$ was initially present in the solution in addition to the major *cis*-**1H$^+$** compound due to occasional warming of the sample during the transfer to the cryostat at 200 K. Subtraction of the normalized spectrum **c** (*trans*-**1H$^+$**) from the initially obtained spectrum (the mixture of *cis* and *trans* species) gave the spectrum of *cis*-**1H$^+$** that is shown in Figure 3.

[39] The *cis*/*trans* isomerization reaction for [Cp*OsH_2(dppe)]$^+$$BF_4^-$ could be studied by IR monitoring of the increase of the ν_{OsH} band of *trans*-**1H$^+$** at 2102 cm^{-1}. In this way the rate constant $k_{250K} = 3.43 \pm 0.03 \times 10^{-4}$ s^{-1} was obtained by plotting $\ln(A_0 - A_t)$ vs. time t (compare to $3.15 \pm 0.02 \times 10^{-4}$ s^{-1} from NMR at 250 K).

[40] N. V. Belkova, M. Besora, M. Baya, P. A. Dub, L. M. Epstein, A. Lledós, R. Poli, P. O. Revin, E. Shubina, *Chem. Eur. J.* **2008**, *14*, 9921–9934.

[41] N. Belkova, M. Besora, L. Epstein, A. Lledós, F. Maseras, E. Shubina, *J. Am. Chem. Soc.* **2003**, *125*, 7715–7725.

[42] The proton affinities of the model [Cp*MH(dhpe)] systems, on the other hand, do not provide the correct basicity order: 255.5 kcal mol^{-1} for **1$_t$** with respect to *cis*-**1$_t$H$^+$**, 258.7 and 257.1 kcal mol^{-1} for the Fe and Ru systems,[28,29] respectively, relative to the model nonclassical [Cp*M(η^2-H_2)(dhpe)]$^+$ complexes.

[43] B. Pleune, R. Poli, J. C. Fettinger, *Organometallics* **1997**, *16*, 1581–1594.

[44] A. Altomare, M. Burla, M. Camalli, G. Cascarano, C. Giacovazzo, A. Guagliardi, A. Moliterni, G. Polidori, R. Spagna, *J. Appl. Crystallogr.* **1999**, *32*, 115–119.

[45] G. M. Sheldrick, *SHELXL97*, *Program for crystal structure refinement*, University of Göttingen, Göttingen, Germany, **1997**.

[46] H. D. Flack, *Acta Crystallogr., Sect. A* **1983**, *39*, 876–881.

[47] L. J. Farrugia, *J. Appl. Crystallogr.* **1997**, *32*, 565.

[48] M. J. Frisch, G. W. Trucks, H. B. Schlegel, G. E. Scuseria, M. A. Robb, J. R. Cheeseman, J. Montgomery, J. A. T. Vreven, K. N. Kudin, J. C. Burant, J. M. Millam, S. S. Iyengar, J. Tomasi, V. Barone, B. Mennucci, M. Cossi, G. Scalmani, N. Rega, G. A. Petersson, H. Nakatsuji, M. Hada, M. Ehara, K. Toyota, R. Fukuda, J. Hasegawa, M. Ishida, T. Nakajima, Y. Honda, O. Kitao, H. Nakai, M. Klene, X. Li, J. E. Knox, H. P. Hratchian, J. B. Cross, C. Adamo, J. Jaramillo, R. Gomperts, R. E. Stratmann, O. Yazyev, A. J. Austin, R. Cammi, C. Pomelli, J. W. Ochterski, P. Y. Ayala, K. Morokuma, G. A. Voth, P. Salvador, J. J. Dannenberg, V. G. Zakrzewski, S. Dapprich, A. D. Daniels, M. C. Strain, O. Farkas, D. K. Malick, A. D. Rabuck, K. Raghavachari, J. B. Foresman, J. V. Ortiz, Q. Cui, A. G. Baboul, S. Clifford, J. Cioslowski, B. B. Stefanov, G. Liu, A. Liashenko, P. Piskorz, I. Komaromi, R. L. Martin, D. J. Fox, T. Keith, M. A. Al-Laham, C. Y. Peng, A. Nanayakkara, M. Challacombe, P. M. W. Gill, B. Johnson, W. Chen, M. W. Wong, C. Gonzalez, J. A. Pople, *Gaussian 03, Revision D.01*, Gaussian, Inc., Wallingford CT, **2004**.

[49] J. P. Perdew, *Phys. Rev. B: Condens. Matter* **1986**, *33*, 8822–8824.

[50] J. P. Perdew, in: *Electronic Structure of Solids* (Eds.: P. Ziesche, H. Eschrig), Akademie Verlag, Berlin, **1991**, pp. 11.

[51] A. D. Becke, *J. Chem. Phys.* **1993**, *98*, 5648–5652.

[52] P. J. Hay, W. R. Wadt, *J. Chem. Phys.* **1985**, *82*, 270–283.

[53] W. R. Wadt, P. J. Hay, *J. Chem. Phys.* **1985**, *82*, 284–298.

[54] A. Höllwarth, M. Böhme, S. Dapprich, A. Ehlers, A. Gobbi, V. Jonas, K. Kohler, R. Stegmann, A. Veldkamp, G. Frenking, *Chem. Phys. Lett.* **1993**, *208*, 237–240.

[55] W. Hehre, R. Ditchfie, J. Pople, *J. Chem. Phys.* **1972**, *56*, 2257–2261.

[56] P. Harihara, J. Pople, *Theor. Chim. Acta* **1973**, *28*, 213–222.

[57] V. Barone, M. Cossi, *J. Phys. Chem. A* **1998**, *102*, 1995–2001.

[58] M. Cossi, N. Rega, G. Scalmani, V. Barone, *J. Comput. Chem.* **2003**, *24*, 669–681.

Received: November 18, 2009
Published Online: February 19, 2010

